Available online at www.sciencedirect.com
SCIENCE DIRECT®
Polymer 44 (2003) 5901–5908
polymer
www.elsevier.com/locate/polymer

Characterisation of the microstructure and deformation of high modulus cellulose fibres

S.J. Eichhorn[a,*], R.J. Young[a], R.J. Davies[b], C. Riekel[b]

[a]*Manchester Materials Science Centre, UMIST/University of Manchester, Grosvenor Street, Manchester M1 7HS, UK*
[b]*European Synchrotron Radiation Facility, B.P. 220, F-38043, Grenoble Cedex, France*

Received 24 March 2003; received in revised form 18 April 2003; accepted 6 May 2003

Dedicated to Prof. Ian M. Ward on the occasion of his 75th birthday

Abstract

This paper reports on the microstructure and deformation of one type of high modulus cellulose fibre characterised using the techniques of Raman spectroscopy and synchrotron X-ray diffraction and it compares this fibre to a lower modulus conventional viscose fibre. The crystallinity of the fibres has been determined using X-ray diffraction. The orientation parameter has been determined by measuring the width of the (200) equatorial reflections for each fibre using microfocus synchrotron radiation and it has also been shown that the crystal orientation parameter varies from the skin to core of the fibres and is different for each type. Mechanical properties of the fibres are reported and it is shown that the high modulus cellulose fibres have very different stress–strain behaviour to the viscose fibres. Finally, it is shown for the high modulus fibre that the 1414, 1260, 1095 and 895 cm^{-1} Raman bands shift under the application of tensile deformation towards a lower wavenumber with the 1095 cm^{-1} band giving information about the backbone chain stretching of the cellulose. The viscose fibres show less significant shifts in this peak. The crystal modulus of the high modulus cellulose fibre has also been determined by calculating the change in the *c*-spacing upon the application of tensile deformation to individual cellulose monofilaments. This change in the *c*-spacing is determined from the change in position of the (002) meridional reflection giving a crystal modulus of 77 GPa. This value is a little low compared to other published data, and reasons for this are discussed. The shear modulus between crystallites is also calculated and compared to previously published data.

Keywords: Raman; Cellulose; X-ray diffraction

1. Introduction

Regenerated cellulose fibres have been made historically by a variety of processes to give desired properties, be it low strength and high extensibility or high strength with low extensibility [1]. In this paper we report findings on the structure and mechanical properties of a fibre based on a process that involves spinning from an anisotropic solution in phosphoric acid using an air gap [2,3]. This work builds upon previously published data [2] by the addition of the use of Raman spectroscopy and synchrotron X-ray diffraction using single fibres to determine their microdeformation, orientation and crystal modulus.

Raman spectroscopy has been used to investigate the deformation micromechanics of conventional man-made polymeric fibres [4] and more recently for the deformation of commercial Cordenka™, Lyocell™ and Enka Viscose™ cellulose fibres [5–7]. The technique relies on the fact that Raman peaks, corresponding to vibrations of structural groups within the polymer chain, shift towards a lower wavenumber upon tensile deformation [4]. This shift, first demonstrated for single polydiacetylene crystals [9], has been shown to be due to the direct deformation of the bonds within the structure [8]. In the case of regenerated cellulose fibres it has been shown that the 895 cm^{-1} [5,6] and 1095 cm^{-1} [5–7] bands both shift towards a lower wavenumber upon tensile deformation. These bands are thought to correspond to vibrations involving heavy atoms (CCC, COC, CHO) [10] and the ring stretching or heavy atom modes (CC, CO) of cellulose [10–12], respectively. However, another plausible assignment for the highest intensity peak at 1095 cm^{-1} includes the β-1,4 glycosidic linkage (C–O–C) between the glucose rings of the cellulose chains [13]. Finally, the bands found at 1275–1292 and

* Corresponding author. Tel.: +44-161-200-3636; fax: +44-161-200-5982.
E-mail address: stephen.j.eichhorn@umist.ac.uk (S.J. Eichhorn).

0032-3861/03/$ - see front matter © 2003 Elsevier Ltd. All rights reserved.
doi:10.1016/S0032-3861(03)00540-8

1406–1407 cm^{-1} for cellulose-I fibres have been assigned to heavy atom stretching (CC, CO) and HCC, HCO and HOC bending, respectively [11].

X-ray diffraction studies of cellulose fibres have also been undertaken to determine, amongst other things, the crystal modulus. Most measurements of the crystal modulus of cellulose have been carried out by loading bundles of fibres and recording changes in the crystallographic *c*-spacing using X-ray diffraction [14,15] and give values in the range 90–110 GPa. Radial texture mapping of cellulose-II fibres has also been conducted using electron diffraction and lateral birefringence applied to sectioned fibre samples [2]. This study showed that there are differences between viscose-type and anisotropic phosphoric acid derived fibre samples and identified the likely 'crack-directions' in the cellulose-II structure [2].

2. Experimental

2.1. Materials

The new fibre investigated was fibre B, a commercial high-modulus cellulose fibre developed by ACORDIS using liquid crystalline cellulose dissolved in phosphoric acid to form an anisotropic solution [16]. The other fibre investigated was a low-modulus Enka-Viscose™ produced by ACORDIS. Both fibre samples were supplied in a continuous filament form.

2.2. Microstructure of fibres determined using X-ray diffraction and Raman spectroscopy

X-ray diffraction characterisation of the fibres was carried out at the European Synchrotron Radiation Facility (ESRF) on beamline ID13 (micro-focus beamline). The beamline was configured with the beam stopped down to a 3 μm spot size and a MARCCD detector was used to collect diffraction images from single fibres. A specimen-to-film distance of 86 mm was used and this was calculated by coating a fibre with some Al_2O_3 powder.

To determine the magnitude of the orientation parameter $\langle \sin^2\theta \rangle$ of the crystalline cellulose across the fibre widths, a batch peak-fitting application was used written in Visual Basic, which is capable of calculating this parameter directly from azimuthal intensity data. The orientation parameter is defined by the equation [17–19]

$$\langle \sin^2\theta \rangle = \frac{\int_0^{\pi/2} \rho(\theta)\sin^3\theta \mathrm{d}\theta}{\int_0^{\pi/2} \rho(\theta)\sin\theta \mathrm{d}\theta} \quad (1)$$

where $\rho(\theta)$ is the distribution of the orientation angle θ relative to the fibre axis, measured directly from the azimuthal spreading of the equatorial reflections. Therefore $\rho(\theta)\sin\theta \mathrm{d}\theta$ is the fraction of segments with an orientation angle between θ and $\theta + \mathrm{d}\theta$ [18]. To find the value of $\langle \sin^2\theta \rangle$, the integrated intensity plots were fitted with a Lorentz-IV function [17]. This was in order to reduce the influence of background noise in the diffraction patterns at high angles (when the sine of the angle is close to unity). For perfect crystallite orientation $\langle \sin^2\theta \rangle = 0$, i.e. the value of the crystal orientation parameter $\langle \sin^2\theta \rangle$ decreases as the degree of crystallite orientation increases. This procedure has been used to successfully determine the orientation parameter within single PBO (poly-*p*-phenylene benzobisoxazole) fibres [20].

A 20° azimuthal cake was taken, ±2° either side of the (200) reflections, for each fibre to determine the peak positions from the beam centre. For subsequent measurements of the peaks a 3 pixel azimuthal scan was taken and the intensities were averaged for each set of data points. Undeformed fibre samples were scanned across their width using a step size of 2 μm with an exposure time of 30 s per measurement.

To determine the crystallinity of the fibres, a number of filaments was secured to a stub and placed within the chamber of a Philips X'PERT APD powder X-ray diffractometer (wavelength = 1.54 Å, Cu K_α radiation). The sample was then scanned from $2\theta = 5$ to 100° in steps of 0.02°. The specimen was also rotated within the X-ray diffractometer chamber to overcome problems of preferred orientation. The resultant graphs were printed out on the Origin™ graph plotting package and the amorphous background areas were determined by weighing. The degree of crystallinity was taken as the ratio of the weight of the crystal peaks to the whole area i.e. crystal peaks plus background [22].

A Renishaw 1000 Raman Imaging Microscope was used in order to record the spectra of the cellulose fibres. Spectra were obtained from individual cellulose monofilaments at 23 ± 1 °C and 50 ± 5% relative humidity. A low power of 25 mW He–Ne laser (633 nm) was used with an intensity of about 1 mW when focused on the monofilament to a spot diameter of about 2 μm. The back-scattered light was collected by the microscope objective (×50 magnification). The laser excitation line is removed by a holographic notch filter, after which the resultant spectrum is produced by a diffraction grating. A highly sensitive Peltier-cooled charge-couple device (CCD) detector is used to record the spectra. The Renishaw software, with a PC computer was used to control the whole system, and to display and process data.

2.3. Mechanical properties of fibres

The mechanical properties of fibre B [2] were determined using an Instron 1121 universal testing machine following the recommendations given in ASTM D3379-75. Single filaments were mounted across a cardboard window using Ciba-Geigy HY/LY 1927 two-part cold-curing epoxy resin.

A minimum of 48 h was allowed for the adhesive to set completely at 23 °C, prior to testing to minimise slippage errors. A gauge length of 50 mm was employed and specimens were tested at a constant rate of $1.67 \times 10^{-3}\ s^{-1}$, with the cross-head speed being $5\ mm\ min^{-1}$. A full-scale load of 1 N was used and minimum of 20 specimens of each fibre type were tested. The testing was undertaken in a controlled laboratory atmosphere of 23 ± 1 °C and 50 ± 5% relative humidity. To calculate the stress in the fibres it was assumed that the fibres all had approximately circular cross-sections. This is thought to be a reasonable assumption as the random measurements of diameters of individual filaments measured in an XL-30 Phillips FEG-SEM (Field Emission Gun Scanning Electron Microscope) showed no significant variations along their lengths. Values obtained for fibre B and the viscose fibre are illustrated in Table 1.

2.4. Micromechanical properties of fibres using Raman spectroscopy and X-ray diffraction

Using the Raman system described in Section 2.1 spectra were again obtained from individual cellulose monofilaments at 23 ± 1 °C and 50 ± 5% relative humidity. Fibres with a gauge length of 50 mm were fixed using cyanoacrylate adhesive on a deformation rig. The axes of the fibres were aligned parallel to the plane of polarisation of the incident laser beam to within ±5°. The monofilament was stretched to failure in steps of the order of 0.5% or less, and this set-up allowed a precision of strain measurement of ±0.05%. Each step required 150 s, which included 120 s for exposure and 30 s for the focusing. Fibre stress was recorded using a purpose-built rig, housing a load cell with a full-scale load of 1 N. This load cell was attached to a transducer, which recorded the load. The precise positions of peaks were located using a Lorentzian curve-fitting algorithm based on the work of Marquardt [23].

For the synchrotron X-ray diffraction deformation studies upon fibre B a customised single fibre loading rig was used to strain the samples. Fibre cards (with a fibre of gauge length 50 mm), with a single monofilament glued with epoxy at each end, were secured to the loading mounts using cyanoacrylate adhesive. Samples were deformed in 200 μm steps (0.4% strain) and diffraction patterns recorded using an exposure time of 30 s and each sample was strained until fracture occurred. Analysis of the results was undertaken using the Fit2D software application, version 10.95 [24,25].

Table 1
Mechanical properties of fibre B and viscose fibres

Fibre	d (μm)	E (GPa)	σ_f^* (GPa)	ϵ_f^* (%)
Fibre B	12.7 ± 0.4	41.71 ± 0.20	1.02 ± 0.13	5.79 ± 0.76
Viscose [6,7]	18.0 ± 0.7	9.40 ± 0.71	0.22 ± 0.05	17.2 ± 1.31

d, Fibre diameter; E, Young's modulus; σ_f^*, breaking stress and ϵ_f^*, breaking strain.

To determine the crystal modulus of fibre B, it was necessary to use caking functions, which allow for intensity integration in the radial direction. This locates the precise position of the meridional reflections (002) and therefore allows the change in the crystal lattice spacing to be monitored with strain. Once the peak positions had been determined in this manner at all load levels, diffraction grating theory was used in order to calculate the c-spacing using the following equation [21,22]

$$c = \frac{n\lambda}{\sin\left(\tan^{-1}\left(\frac{x}{r}\right)\right)} \quad (2)$$

where n is the reflection index, λ is the radiation wavelength, x is the reflection vertical height on the pattern and r is the specimen to film distance determined using the method described in Section 2.1. By defining the change in the c-spacing as a ratio of the initial c-spacing as the crystal strain, then by plotting this as a function of the applied stress as done by Sakurada et al. [14] one can determine the crystal modulus from the gradient of the curve (assuming that the stress on the crystals is the same as that on the fibre as a whole, i.e. 'uniform stress').

3. Results and discussion

3.1. Microstructure of fibres

Typical X-ray diffraction patterns are shown in Fig. 1(a) and (b) for single fibres of sample B and viscose, respectively. It is clear that the equatorial reflections (110)/(200) for the viscose fibres are more diffuse than for fibre B suggesting that this sample has a lower crystal orientation. Indeed all reflections in pattern of fibre B are much sharper indicating a more highly crystalline sample. A diffractometer scan of the diffraction pattern for fibre B is shown in Fig. 2. The peaks for the fibre B sample are clearly defined, intense and have a low amorphous background. The crystallinity of fibre B was found to be 65.1 ± 0.4%, which compared to a value of 19.6 ± 1.3% for the viscose sample. The much higher value of crystallinity for fibre B is found since the spinning process involves liquid crystalline cellulose [16], and this could also be a contributing factor to its high modulus as will be discussed in Section 3.2.

The values of the orientation parameter across the fibre widths for fibre B and viscose fibres were determined by using synchrotron X-ray diffraction as outlined in Section 2.1. The intensity plots were fitted using a Lorentz function as described in Section 2.1 and a typical curve fit is shown in Fig. 3. To determine the positions of the peaks, before determining the orientation distributions, it was necessary to fit the equatorial (200) peak, along with two other nearby peaks (also with Lorentz functions) as is reported in Fig. 4. One can see from Fig. 4 that there is a good correlation between the data and the fitting function. A comparison for

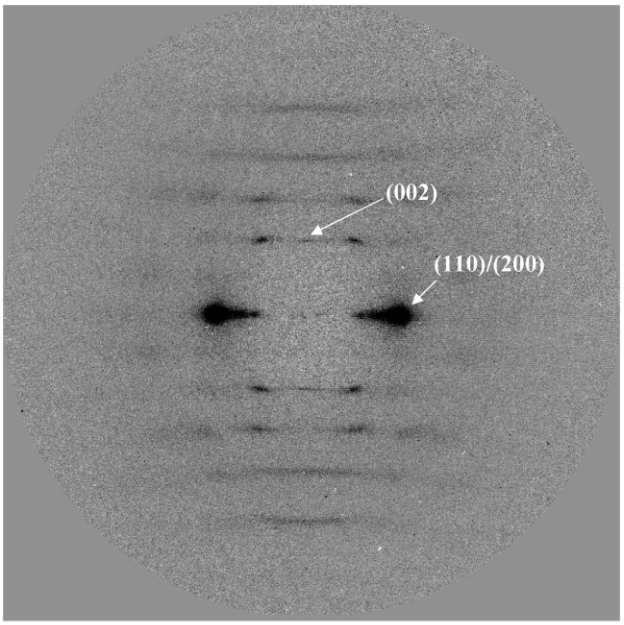

(a)

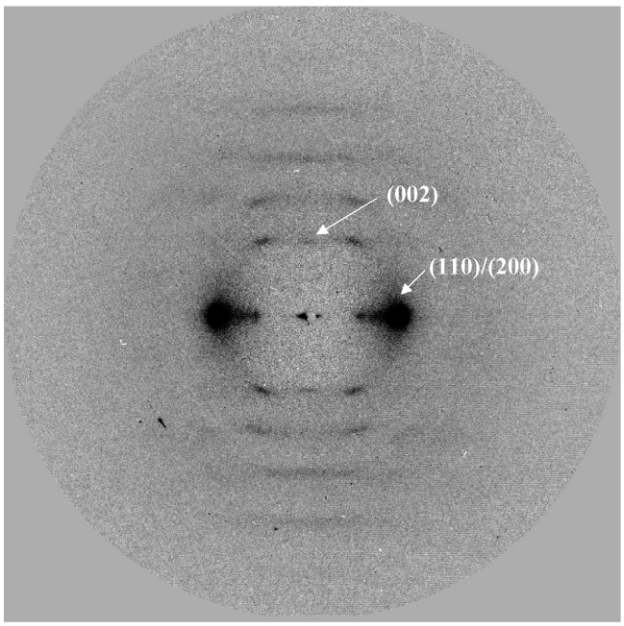

(b)

Fig. 1. Synchrotron X-ray diffraction patterns for monofilaments of (a) fibre B and (b) viscose fibres indicating the positions of the (110)/(200) and (002) reflections.

both fibre B and viscose orientation parameter distributions is shown in Fig. 5. It is clear that fibre B has higher overall orientation than the viscose fibres, and that it also has a more uniform distribution from the skin of the fibre to the core. It is also apparent from Fig. 5 that the viscose fibres have a higher orientation at the skin of the fibres than at the core. This can be explained in terms of the spinning process where the shear forces on the outer regions of the filament during processing induce higher orientation. An explanation

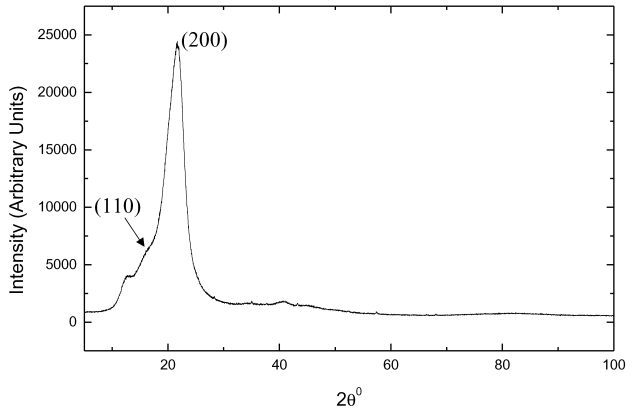

Fig. 2. Variation of intensity with 2θ for a sample of fibre B indicating the positions of the (200) and (110) reflections.

for differences between the fibres in terms of their orientation distributions could be that they are manufactured in different ways.

A typical Raman spectrum for fibre B is shown in Fig. 6 indicating peaks located at 895, 1095, 1260, 1368 and 1414 cm^{-1}. All bands apart from the 1414 cm^{-1} may be assigned to bond vibrations that are associated with main chain segmental stretching modes [10–14]. However, the 1414 cm^{-1} is associated with 3-atom bond vibrations (HCC, HCO and HOC bending) that ought to be influenced by transverse forces through side-chain hydrogen bonding. It was noted that the Raman spectra obtained for the fibre B samples were much more clearly defined than those obtained for the viscose sample [6,7] which again is a reflection of their more ordered structure.

3.2. Mechanical properties of fibres

A typical stress–strain curve obtained for fibre B compared with a typical viscose fibre (as previously reported [6,7]) is shown in Fig. 7. It is clear that fibre B has high strength (>1 GPa) as has previously been reported [2]. It also exhibits an initially steep linear region up to 1%

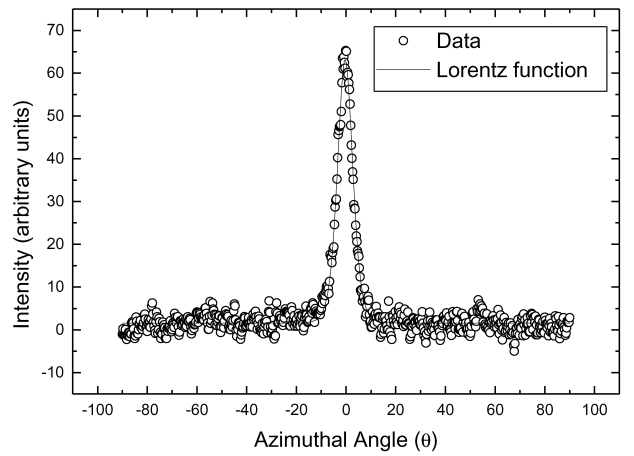

Fig. 3. Demonstration of the intensity of the azimuthally integrated (200) reflection with angle of fibre B cellulose and subsequent peak fitting.

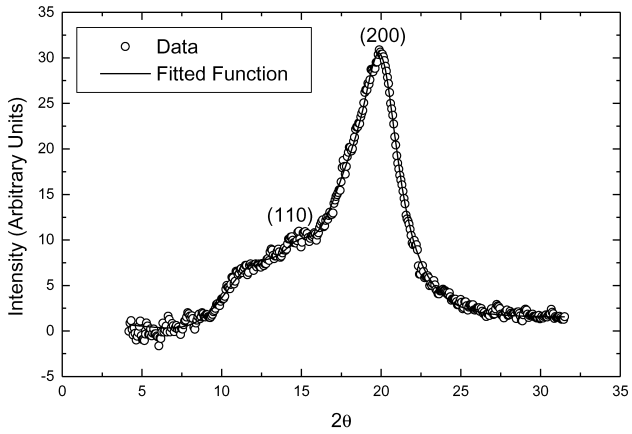

Fig. 4. Example of a Lorentz fitting function used to determine the positions of the (200) equatorial reflections for orientation parameter determinations.

strain, after which there is a yield point and a subsequent steep strain-hardening region. However, the viscose fibre shown in Fig. 7 also has an initial linear region with a yield point at 1% strain, but exhibits less strain-hardening as has been previously reported [6]. The mechanical properties of these two types of fibre are reported in Table 1. It is clear that fibre B has a much higher initial modulus than the viscose fibres, indicating that their microstructure is significantly different as has been confirmed from the X-ray diffraction of the fibres in Section 3.1. Higher overall orientation of the fibre B samples therefore has an influence on the improved mechanical properties compared to the viscose fibres. The values obtained for fibre B are also of the same order of magnitude as those obtained in another study by Northolt et al. [2].

3.3. Fibre micromechanics

Some of the Raman peaks labelled in Fig. 6 for the fibre B samples were found to shift with tensile deformation. It was not possible to record peak shifts in peaks, other than for the 1095 cm^{-1} band, for the viscose fibres since the

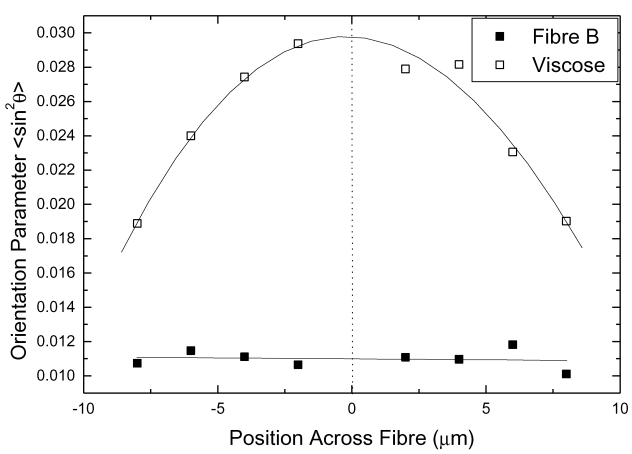

Fig. 5. Orientation parameter distributions for fibre B and viscose samples from the centre (dotted line) to the fibre-skin.

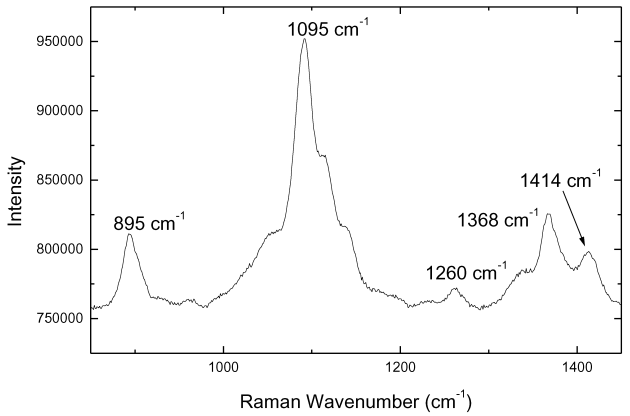

Fig. 6. A typical Raman spectrum for a single monofilament of fibre B indicating the positions of the 895, 1095, 1260, 1368 and 1414 cm^{-1} peaks.

spectra contained considerably more noise. Examples of such shifts are shown in Fig. 8(a)–(c). It is clear from Fig. 8(c) that the 1368 cm^{-1} peak does not appear to shift and similar behaviour was found for the 1260 cm^{-1} band. If the peak positions are plotted as a function of strain then it is easier to observe this effect as shown in Fig. 9. These Raman peak shifts towards a lower wavenumber are thought to correspond to the direct deformation of bonds within the cellulose chain structure as predicted theoretically for polydiacetylene single crystals [8]. All the peaks are shown to shift to a lower wavenumber non-linearly with strain reflecting the non-linear stress–strain curve for fibre B in Fig. 7. The 1414 cm^{-1} peak (assigned to HCC, HCO and HOC bending [11]) has a higher band shift rate to the three main-chain assigned peaks (895, 1095 and 1260 cm^{-1}). There is a significant Raman band shift of the 1414 cm^{-1} peak implying that the hydrogen bonding within the structure plays a significant role in stress-transfer between adjacent cellulose chains.

The highest intensity Raman peak at 1095 cm^{-1} has been shown previously to shift towards a lower wavenumber and to be most indicative of the molecular deformation of cellulose fibres [5–7]. The detailed Raman band shift deformation curves for this peak, for fibre B and viscose, are

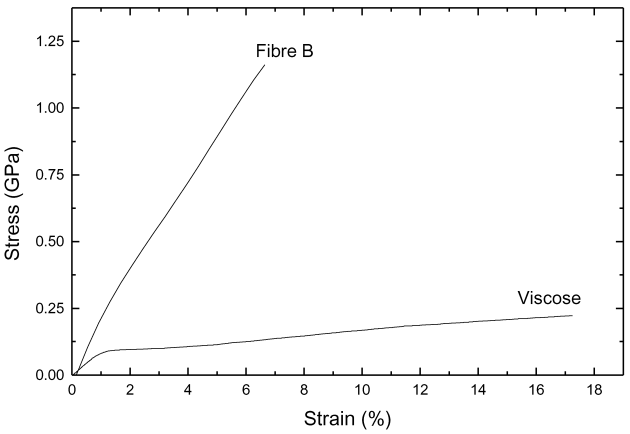

Fig. 7. Typical stress–strain curves for fibre B and viscose fibres [6,7].

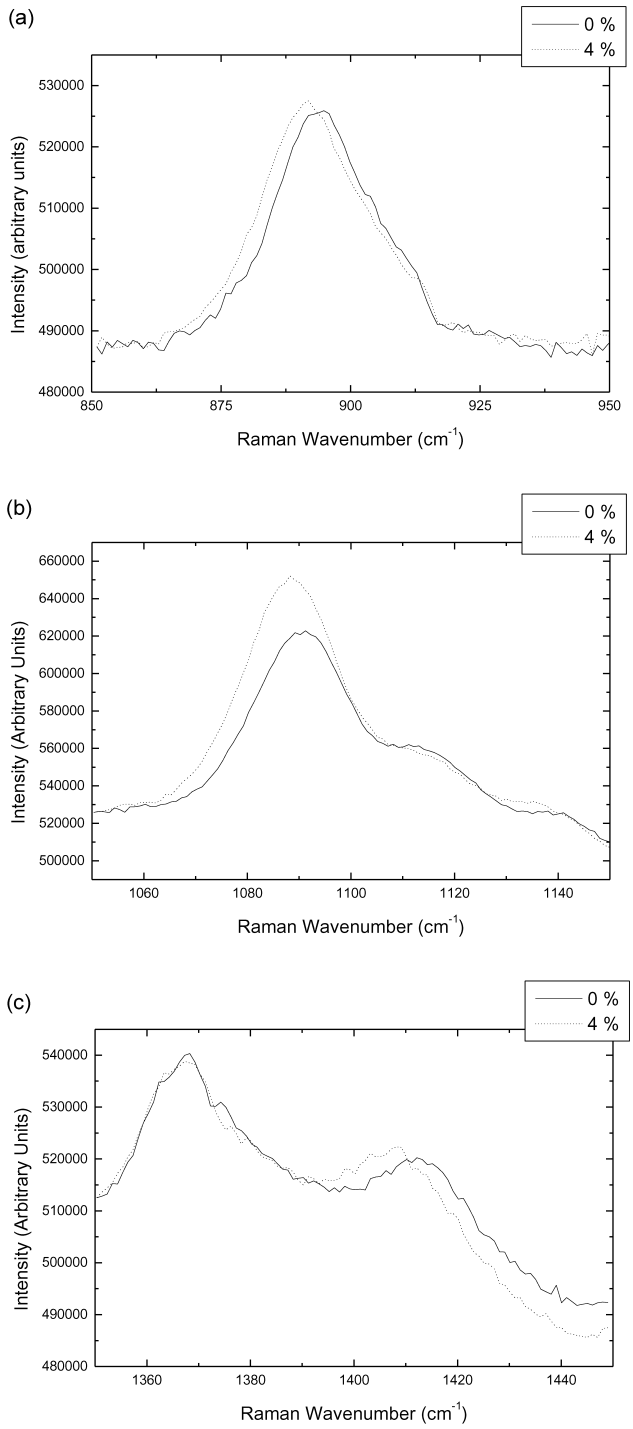

Fig. 8. Shifts with fibre strain for the Raman bands at (a) 895, (b) 1095, (c) 1414 cm^{-1}.

shown in Fig. 10(a) and (b) for strain and stress, respectively. From Fig. 10(a) where the Raman shift is plotted against strain, one can see that the data reflect the stress–strain curve for fibre B as shown in Fig. 7. This could be because the modulus of fibre B is large, and hence the translation of fibre deformation to molecular deformation is likely to be less influenced by local microstructure. It is also noted that the shift with respect to strain for the viscose

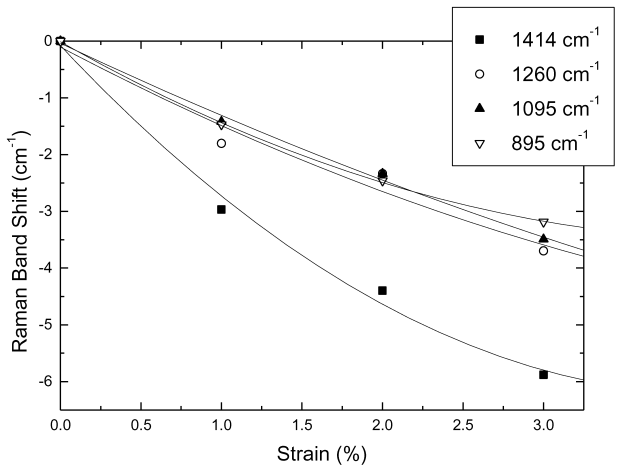

Fig. 9. Typical Raman band shifts with respect to strain for the 895, 1095, 1260 and 1414 cm^{-1} peaks. The fitted solid lines are third order polynomials.

fibres is barely detectable. This is due to the fact that the 1095 cm^{-1} Raman band shift within cellulose fibres has been shown to be controlled by the stress on the fibres [5,7]. Therefore, since the viscose fibre deforms to high strains

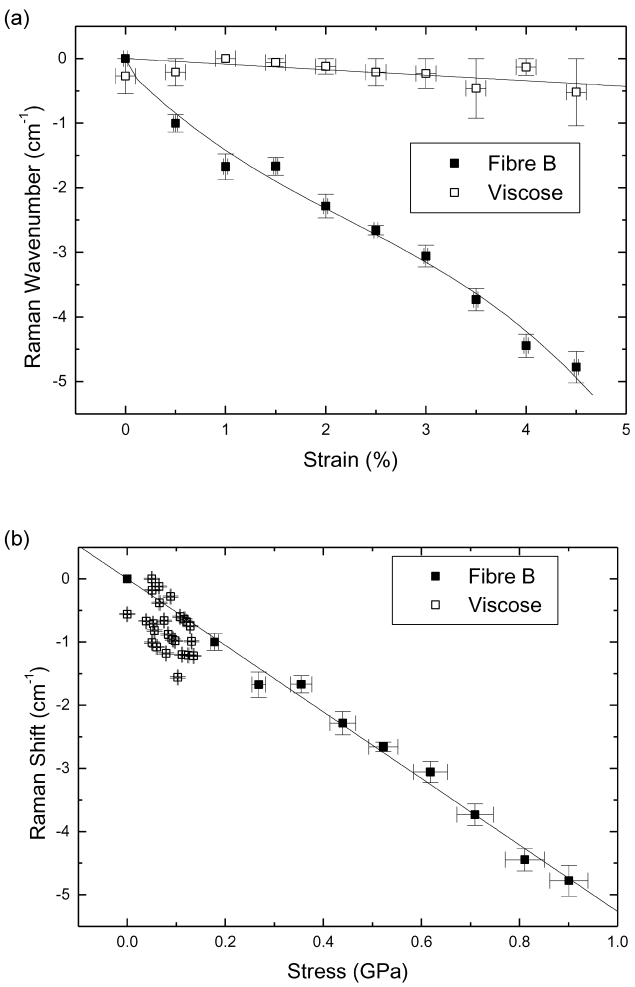

Fig. 10. Raman band shifts with respect to (a) strain and (b) stress for the 1095 cm^{-1} peak for fibre B and viscose.

(Fig. 7) with little increase in stress, then small shifts in this peak are expected. However, when the Raman band shifts are plotted as a function of stress one can see from Fig. 10(b) that for both fibres there is a good correlation with a linear regression. This is observed because previous studies [5–7] have shown that the microstructure of regenerated cellulose fibres leads to uniform stress upon the crystals in the structure. The shift rates with respect to strain and stress for fibre B and viscose are reported in Table 2. The values for fibre B are significantly higher than those previously reported for other regenerated cellulose fibres (including the viscose fibre discussed in this paper) produced by different processes [6,7]. The exact reasons for this are unclear, but it could possibly be due to the fact that the microstructures of these fibres differ as is clear from the X-ray diffraction patterns (Fig. 1(a) and (b)).

A crystal modulus determination was attempted for both fibre types, but the viscose fibres did not give a clear enough meridional reflection at (002) for peak fitting purposes and fibre damage from the X-ray beam caused premature failure of the samples. For the crystal modulus determination for fibre B it was necessary to fit meridional reflections with Voigt functions as described in Section 2.3. An example of a fit to these peaks is given in Fig. 11. The scattering on other layer lines was found to be too weak in intensity for reasonable fits to the data to be made and therefore only the reflection at (002) was used in the analysis of the data. The crystal modulus determination for fibre B is reported in Fig. 12. Firstly, it must be noted that radiation damage to the cellulose fibres, a well-documented effect [26], meant that premature failure of the samples occurred and therefore only three data points are plotted. The values obtained were 77 ± 5 GPa for the (002) meridional reflection. This value is low compared to figures of 90 and 106 GPa obtained for other experimental determinations of the crystal modulus of cellulose-II [14,15]. However, one must take into account damage to the fibres, which may be one reason why a smaller value has been obtained. However, if one takes the ratio of the fibre B modulus to the crystal modulus, as was reported in another study [2], then one obtains a value of 0.5. This is of the same order as figures calculated from similar data obtained for HM PBO (high modulus poly-*p*-phenylene benzsobisoxazole) fibres [21]. This is in agreement with the previous study of fibre B [2] underlying the similarity between its microstructure and morphology with that of PBO that has been noted before [2].

Table 2
Raman band sensitivities for fibre B and viscose cellulose fibres

Fibre	$d\nu/d\varepsilon$ ($cm^{-1}/\%$)	$d\nu/d\sigma$ (cm^{-1}/GPa)
Fibre B	-1.08 ± 0.03[a]	-5.26 ± 0.08
Viscose [6,7]	-0.06 ± 0.02[a]	-4.89 ± 2.09

$d\nu/d\varepsilon$ and $d\nu/d\sigma$ are the rates of Raman shift with strain and stress, respectively.
[a] Mean rates with respect to strain.

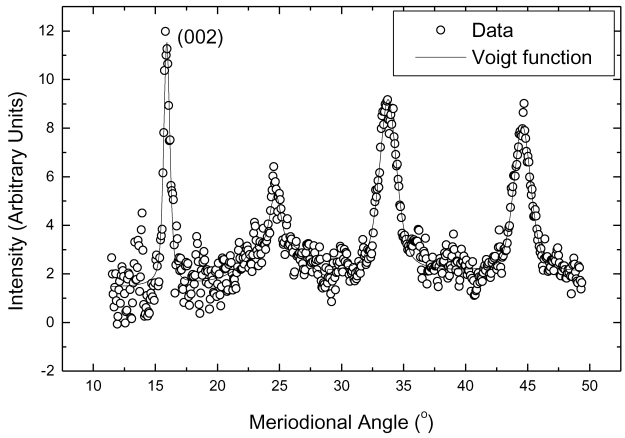

Fig. 11. Typical peak fits used to determine the crystal modulus of the fibre B sample using the meridional reflection (002) and subsequent layer lines.

3.4. Calculation of the shear modulus of crystalline domains for cellulose

The shear modulus of crystalline domains, g, has been found to be related to the chain modulus of fibres (E_c), the fibre modulus (E) and the second moment of the orientation parameter $\langle \sin^2 \Theta \rangle_E$ by the equation [18]

$$\frac{1}{E} = \frac{1}{E_c} + \frac{\langle \sin^2 \Theta \rangle_E}{2g} \quad (3)$$

This equation is commonly known as the linear series aggregate model [18] and has been demonstrated to describe the structure cellulose fibres [6,7]. The second moment of the orientation parameter differs from the orientation parameter used in this study and in that an isotropic sample yields a value of $\langle \sin^2 \Theta \rangle_E$ equal to 0.5 and for the standard definition this is 2/3 [26]. These differences shall be ignored for the sake of this calculation since the values can be approximated to within 10% of the second moment parameter below values of about 0.25 [27]. If one takes the orientation parameters for the centres of fibre B and

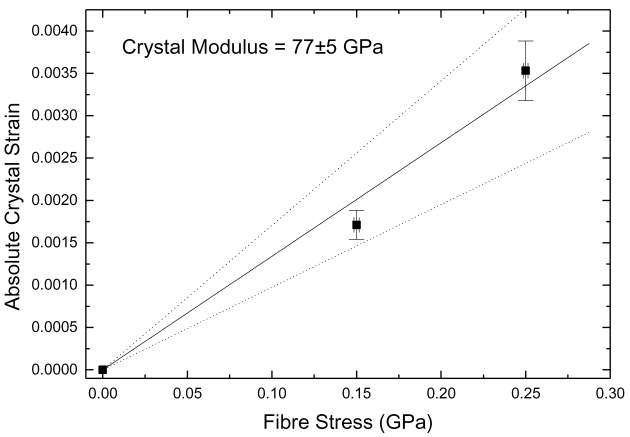

Fig. 12. Calculated crystal strain with applied fibre stress for fibre B for the (002) meridional reflection. Dotted lines indicate the 95% confidence bands.

viscose samples to be 0.013 and 0.029, respectively (from Fig. 5) then one obtains shear modulus (g) values of 0.60 and 0.15 GPa for fibre B and viscose, respectively (using $E_c = 77$ GPa from Section 3.3). These are lower values than those obtained by Northolt et al. [2] for fibre B ($2.4 \leq g \leq 3.8$ GPa) using dynamic testing, probably due to the difference in testing rate. It appears from this analysis that the considerably higher modulus of fibre B compared to the viscose sample is due to a combination of both a higher level of crystal orientation and shear modulus.

4. Conclusions

The use of X-ray diffraction has shown that the fibre B and viscose samples have different microstructures in terms of their crystallinities and the distribution of their orientation parameter determined across the widths of the filaments. The orientation was found to be much greater for the fibre B sample than for the viscose fibres. This is reflected in the much higher modulus and strength values obtained for this fibre suggesting that its higher crystal orientation contributes towards this increase. The fibre B cellulose sample also has a much more uniform orientation across its width, which is a desirable property if one wishes to maximise mechanical properties. The Raman technique for determining the molecular deformation of high modulus cellulose fibres is demonstrated and it is shown that with strain, the shift profile reflects the non-linear stress–strain curve of fibre B. However, a comparatively small shift is observed in the viscose fibres due to its low modulus, as a result of lower orientation. The crystal modulus of the fibre B sample is also determined using synchrotron X-ray diffraction, and it was found that lower values were obtained than by other studies on fibre bundles. This may be due to beam damage as the fibres were observed to break prematurely. The shear modulus has been calculated from a linear series aggregate model, and found to be an order of magnitude lower if the Young's modulus is used in the calculation. However, values in agreement with previous studies of fibre B are obtained if the dynamic modulus is used instead.

Acknowledgements

Two authors (S.J.E., R.J.Y.) wish to thank the EPSRC for funding the work (Grant No. GR/M82219). The authors would also like to thank Dr Hanneke Boerstoel, Dr Mauritis Northolt and ACORDIS for supplying fibre samples. We would also like to thank Dr Andrew Hammersley for use of the Fit2D software application.

References

[1] Gordon-Cook J. Handbook of textile fibres II. Man-made fibres, 5th ed. Durham: Merrow Publishing Co. Ltd; 1984. Chapter 1.
[2] Northolt MG, Boerstoel H, Maatman H, Huisman R, Veurink J, Elzerman H. Polymer 2001;42(19):8249–64.
[3] Boerstoel H. Liquid crystalline solutions of cellulose in phosphoric acid. PhD Thesis, University of Groningen; 1998.
[4] Young RJ. J Text Inst 1995;86:360–81.
[5] Hamad WY, Eichhorn SJ. ASME J Engng Mat Tech 1997;119:309–13.
[6] Eichhorn SJ, Young RJ, Yeh WY. Text Res J 2001;71:121–9.
[7] Eichhorn SJ, Sirichaisit J, Young RJ. J Mat Sci 2001;36:3129–35.
[8] Batchelder DN, Bloor D. J Polym Sci—Polym Phys Edn 1979;17:569–81.
[9] Mitra VK, Risen Jr. WM, Baughman RH. J Chem Phys 1977;66:2731–6.
[10] Atalla RH, Nagel SC. Science 1974;185:522–3.
[11] Wiley JH, Atalla RH. Carbohydrate Res 1987;160:113.
[12] Cael JJ, Gardner KH, Koenig JL, Blackwell J. J Chem Phys 1975;62:1145.
[13] Edwards HGM, Farwell DW, Webster D. Spectrochimica Acta Part A 1997;53:2383.
[14] Sakurada I, Nukushina Y, Ito T. J Polym Sci 1962;57:651–60.
[15] Matsuo M, Sawatari C, Iwai Y, Ozaki F. Macromolecules 1990;23:3266–75.
[16] Boerstoel H, Maatman H, Westerink JB, Koenders BM. Polymer 2001;42:7371–9.
[17] Northolt MG. Polymer 1980;21:1199–204.
[18] Northolt MG, Baltussen JJM. J Appl Polym Sci 2002;583:508–38.
[19] Northolt MG, Van Aartsen JJ. J Polym Sci—Polym Symp 1977;58:283–96.
[20] Davies RJ, Montes-Morán MM, Riekel C, Young RJ. J Mater Sci 2003;38:2105–15.
[21] Davies RJ, Montes-Morán MM, Riekel C, Young RJ. J Mater Sci 2001;36:3079–87.
[22] Young RJ, Lovell PA. Introduction to Polymers, 2nd ed. London: Chapman and Hall; 1991. Chapter 4.
[23] Marquardt DW. J Soc Ind Appl Math 1963;11:431.
[24] Hammersley AP. ESRF Internal Report, ESRF97HA02T. Fit2D: an introduction and overview; 1997.
[25] Hammersley AP, Riekel C. Sync Rad News 1989;2:24–6.
[26] Klemm D, Phillip B, Heinze T, Heinze U, Wagenknecht W. Comprehensive cellulose chemistry. Fundamentals and Analytical Methods, vol. 1. Weinheim: Wiley; 1998.
[27] Baltussen JJM. Tensile deformation of polymer fibres. PhD Thesis, Technical University of Delft; 1996.